



Numerical Simulation of Inclusion Collision Growth and Removal in a Tundish with Intermittent Induction Heating

BIN YANG ^{1,4} HONG LEI,² and DAZHAO GOU^{3,5}

1.—School of Materials and Metallurgy, University of Science and Technology Liaoning, Anshan 114051, People's Republic of China. 2.—Key Laboratory of Electromagnetic Processing of Materials, Ministry of Education, Northeastern University, Shenyang 110819, Liaoning Province, People's Republic of China. 3.—School of Chemical Engineering, University of New South Wales, Sydney, NSW 2052, Australia. 4.—e-mail: yang583766560@163.com. 5.—e-mail: d.gou@unsw.edu.au

To explore the effect of intermittent induction heating mode on inclusions in the tundish, a three-dimensional coupled electromagnetic field, flow field and inclusion field were developed. Numerical results show that medium frequency medium heating and medium frequency medium pause mode and head-to-tail long heating mode are beneficial to the removal of inclusions in the channel. At the same time, these two induction heating modes can not only help the macroscopic transmission and collision growth of inclusions but also help the removal of inclusions, which are two very good induction heating modes. The overall order of magnitude of the turbulent collision source term during induction heating is one order of magnitude higher than that of the turbulent collision source term without induction heating, and the difference within the channel is nearly two orders of magnitude, suggesting that the reasonable heating mode and heating time can help maximize the collision growth and removal of inclusions in the channel.

INTRODUCTION

For decades, induction heating technology has been used to melt metals and alloys, particularly nonferrous metals, but for more than 2 decades, it has only been used to heat molten steel in continuous casting tundishes. Industrial tests and online applications have demonstrated that electromagnetic induction technology can effectively compensate for the temperature drop of the molten steel in the tundish and make the temperature homogeneous^{1–6} as well as effectively improve the cleaning of the molten steel in the tundish.^{7–9} Simultaneously, inclusion characteristics have become an important criterion in determining high-quality steel.^{10–12} Numerous metallurgical workers at home and abroad have employed industrial tests, physical simulations, numerical simulations and other methods to investigate the behavior of inclusions in steel

to efficiently remove them. Among these methods, numerical simulation has the advantages of being inexpensive, not being constrained by experimental constraints such as location and high temperature and having high repeatability. Because of advances in computer technology and the maturity of numerical calculation methods, numerical simulation has become a crucial tool for many researchers studying the behavior of inclusions in molten steel.¹³ As a result, by investigating changes in the type, size, number and shape of tundish inclusions, industrial production can be guided to control the behavior of tundish inclusions.^{10–12}

The main mathematical models for the motion behavior of inclusions are heterogeneous models (Lagrangian models and Euler models), homogeneous models (particle collision dynamics models and fractal growth models) and multi-mode mathematical models (multi-scale inclusion number conservation model, inclusion mass and number model, Euler-Lagrangian model) and inclusion nucleation and growth model. Among them, research on inclusions in induction heating tundish focuses on the

following points: (1) research based on the inclusion mathematical model, Euler-Lagrangian model and inclusion number conservation model; (2) research based on different inclusion states, such as radius size, initial state and so on; and (3) numerical calculations and industrial experiments based on different tundish physical models, such as channel diameter size, length, tundish shape and so on.

Based on the above, Ilegbusi et al.¹⁴ employed the inclusion number conservation model to do mathematical computations on a shallow tundish with the electromagnetic field. The results demonstrate that the inclusion removal efficiency in the shallow tundish is quite low in any circumstance. Wang et al.¹⁵ employed the Euler-Lagrangian method to calculate inclusion trajectories in the channel induction heating tundish using the random walk model. The findings suggest that electromagnetic pressure facilitates the clearance of inclusions, particularly bigger inclusions. The inclusion removal rate increased from 67.45% to 96.43% as the power increased from 800 kW to 1200 kW. Turbulent and Brownian collisions become more active as power increases, but Stokes collisions do the opposite. Based on the discrete particle method model, Xing et al.^{16,17} created a three-dimensional mathematical model for a novel induction heating tundish with curved channels. Numerical studies reveal that the tundish with 3 m channel lengths has better flow characteristics than those with 4 m and 2 m channel lengths. Channel lengths of 3 m and 2 m demonstrated good inclusion removal effectiveness; however, channel length of 4 m was inefficient. The new tundish channels have a greater inclusion removal rate than the regular tundish channels. Tang et al.¹⁸ used the Euler-Lagrangian method to calculate inclusion trajectories in a channel induction heating tundish using the random walk model. Numerical calculations reveal that the movement trajectories of inclusion particles of different sizes at the channel exit are different, and larger-sized inclusions are more easily collected and removed by the mold slag layer. Lei et al.¹⁹ performed numerical calculations on a dual-channel induction heating tundish based on the inclusion mass and number conservation models, and the findings revealed that Archimedes collision is also an essential collision mechanism for inclusion coalescence. The inclusion removal rate in the channels is up to one-third that of the tundish, and when channel induction heating is used, the inclusion removal rate in the tundish rises from 21.4% to 35.05%. Dou et al.²⁰ investigated a trough-type induction heating tundish in an industrial application. The results revealed that large inclusions with a diameter $> 9 \mu\text{m}$ were more concentrated along the channel's edge in the induction heating channel. Induction heating has a limited effect on inclusions $< 9 \mu\text{m}$ in diameter. Yi et al.²¹ used the Lagrangian model to simulate inclusions of various diameters in a six-strand T-shaped tundish; the

findings showed that the inclusion clearance rate in the channel gradually declined from 70.9% to 56.1% as the diameter of inclusion particles increased from $10 \mu\text{m}$ to $50 \mu\text{m}$.

As stated in the review, inclusion research mainly concentrates on mathematical models, physical models and industrial experiments. Based on the inclusion mass and number conservation model of inclusion, this paper investigates the inclusion field distribution characteristics under different intermittent induction heating modes and seeks an intermittent induction heating mode that is beneficial to guide production and practice. The main points of innovation are (1) intermittent mode under half-range induction heating mode, which involves exploring a new heating mode and conducting theoretical analysis, and (2) describing and analyzing the physical field of the characteristic zone in the tundish under this mode, which allows for a comprehensive assessment.

PHYSICAL MODEL

Figure 1a depicts the overall view of the tundish grid, while Fig. 1b and c provides detailed dimensional drawings of the tundish to better highlight its geometric properties.

The simulations are conducted to analyze the collision growth and removal behavior of inclusions under four intermittent induction heating modes. The first operating mode is high-frequency short heating and high-frequency short pause mode, the second operating mode is medium-frequency medium heating and medium-frequency medium-stop mode, the third operating mode is mixed, and the fourth operating mode is head-to-tail long heating. The heating mode is shown in Fig. 1d, where the blue area represents the starting of heating, and the blank space indicates the halting of heating. The finite element method is employed to solve Maxwell's equations, from which the electromagnetic force and Joule heat power density are derived. The electromagnetic force is then integrated into the momentum equation, and the Joule heat power density is incorporated into the energy equation for fluid flow analysis. The primary goal is to determine which heating method yields the best inclusion field distribution, characterized by a homogenized inclusion field in the tundish, smaller particle sizes at the tundish exit and a high inclusion removal rate under the energy-saving conditions of half-process induction heating, which conserves half the energy compared to full-process induction heating. Additionally, a comprehensive analysis is conducted, including the particle size, removal rate, and inclusion characteristics in the dead zone. The steel varieties smelted within the induction heating tundish primarily comprise heavy rail steel, automotive steel, cold heading steel, gear steel and high-quality specialty steel, among others, serving as primary targets for smelting. Therefore, the steel

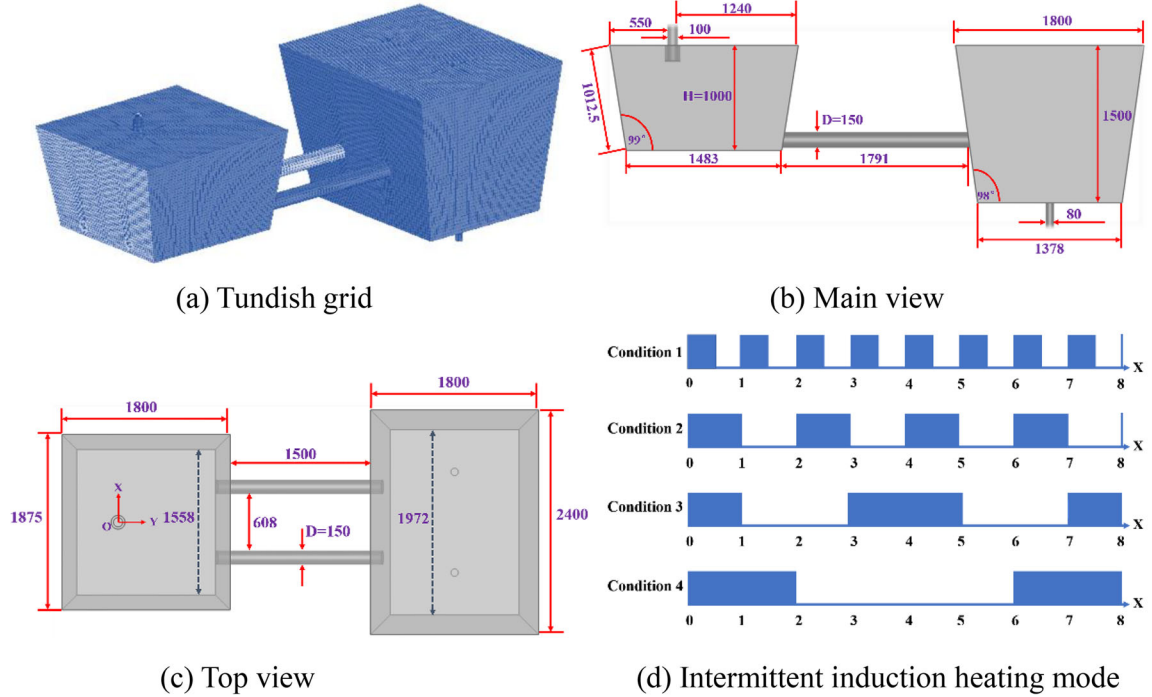


Fig. 1. Model diagram and numerical calculation conditions (length unit: mm).

properties utilized in this study represent universal material characteristics. The density of molten steel satisfies the relationship, $\rho = 8523 - 0.8358 T$ (kg/m^3), the initial temperature is 1800 K, and the thermal conductivity, heat capacity and viscosity of the molten steel are 41 ($\text{W}/(\text{m K})$), 750 ($\text{J}/(\text{kg K})$) and 0.0061 ($\text{kg}/(\text{m s})$), respectively.

MATHEMATICAL MODEL OF INCLUSIONS

Basic Assumptions

The physical model is a simplified version of the tundish found in real industrial induction heating equipment, ignoring the thickness of the tundish wall and simplifying the lamination of silicon steel sheets, etc. The numerical calculation process (1) ignores the effect of furnace liner thickness on heat transmission conditions and (2) the tundish wall surface is smooth. Despite these simplifications and assumptions, the numerical calculation model accurately identifies the key features of industrial tundishes. It can successfully replicate and reflect actual fluid dynamics, heat transfer processes and inclusion dynamic characteristics, giving it significant practical relevance.^{13,23}

Simplifying the transfer behavior of inclusions in the tundish is necessary for some numerical predictions:

- (1) Inclusions are considered to be rigid and inert spherical particles.
- (2) The molten steel has no intention of generating any chemical reactions.
- (3) The inclusion particles remain spherical after

the collision, and their movements are unaffected by one another until the collision aggregation.

- (4) Inclusions are thought to be permanently separated from the molten steel once they come into contact with the tundish wall and the slag surface.

Inclusion Governing Equation

The inclusion collision-coalescence and growth model can be used as follows:¹⁹

$$\nabla \cdot (\rho_f \vec{u}_C C) = \nabla \cdot (\rho_f D_{\text{eff},C} \nabla C) \quad (1)$$

$$\nabla \cdot (\rho_f \vec{u}_N N) = \nabla \cdot (\rho_f D_{\text{eff},N} \nabla N) + S_N \quad (2)$$

where $D_{\text{eff}} = D_0 + \mu_t / \rho_f \text{Sc}_t$, where ρ_f is the fluid density, \vec{u}_f is the fluid velocity, D_{eff} is the effective kinematic diffusivity, \vec{u}_C is the inclusion volume concentration slipping velocity and \vec{u}_N is the inclusion number density slipping velocity, C is the inclusion volume concentration, N is the inclusion number density, D_0 is the molecular diffusion coefficient, μ_t is the turbulence viscosity, and Sc_t is the turbulent Schmidt number.

Collision Source Term

The turbulence collision significantly increases the collision probability of inclusions. The induction heating creates a strong stirring effect in molten steel, forming turbulent flows. These turbulences allow the inclusions to circulate and collide with

each other and the walls, enhancing the probability of their ascent to the surface of the molten steel and thereby their removal. Brownian motion also plays a pivotal role in the removal of smaller inclusions. These microscopic particles undergo random motion due to thermal vibrations, and this oscillation permits them to collide with larger inclusions or bubbles. Consequently, they adhere to the larger entities and are carried along to the liquid surface because of their higher buoyancy. Last, the Stokes collision process also contributes to the removal mechanism. Stokes' law governs the falling or rising velocity of particles in fluid. It states that under gravitational force, the smaller inclusions with less inertia will experience a drag force in proportion to their velocity when colliding with larger inclusions or bubbles. This could make the smaller particles settle down more slowly or even adhere to the larger inclusions or bubbles rising more quickly to the molten steel's surface. Therefore, these three factors together affect the removal of inclusions in steel during an induction heating process. In the electromagnetic field, the movement of inclusions is affected by electromagnetic force and develops into an electromagnetic collision based on Stokes collision. Turbulent and electromagnetic collisions are the main collision modes in the continuous casting process, Stokes collision is the secondary collision mode, and Brownian collision can be ignored.

The collision source term in the inclusion number conservation equation for turbulent collision is:

$$\begin{aligned} S_{\text{turb}} &= \frac{1}{2} \int_0^\infty \int_0^\infty 1.3 \alpha \sqrt{\frac{\pi \rho_f \varepsilon}{\mu_1}} (r_i + r_j)^3 N_i N_j dr_i dr_j \\ &= 2.6 \alpha \sqrt{\frac{\pi \rho_f \varepsilon}{\mu_1}} N^{*2} r^{*3} \end{aligned} \quad (3)$$

The collision source term in the inclusion number conservation equation for electromagnetic collision is:

$$\begin{aligned} S_{\text{Arch}} &= \frac{1}{2} \int_0^\infty \int_0^\infty \left| \frac{2\pi \vec{g} \Delta \rho}{9\mu_1} - \frac{\pi \vec{J} \times \vec{B}}{6\mu_1} \right| \\ &\quad \left| r_i^2 - r_j^2 \right| (r_i + r_j)^2 N_i N_j dr_i dr_j \quad (4) \\ &= \frac{10\pi}{9\sqrt{6}} \left| \frac{\frac{3}{4} \vec{J} \times \vec{B} - \vec{g} \Delta \rho}{\mu_1} \right| N^2 r^{*4} \end{aligned}$$

where S_{turb} is the reduction in the number density of inclusions caused by turbulent collision per unit time, $1/(\text{m}^3 \text{ s})$, S_{Arch} is the reduction in the number density of inclusions caused by electromagnetic collision per unit time, $1/(\text{m}^3 \text{ s})$, \vec{g} is the gravitational acceleration, r^* is the characteristic inclusion radius, μ_1 is the kinematic viscosity, ε is the turbulent kinetic energy rate, α is the coagulation coefficient of particle, \vec{B} is magnetic flux density, \vec{J}

is the induced current density, subscripts (i, j) indicating the correlation between particles of sizes r_i and r_j , π are constant, and $\Delta \rho$ is the density difference between inclusions and molten steel.

Boundary Conditions

The adsorption formulae for the volume concentration and number density of inclusions for the tundish wall are:¹⁹

$$J_{\text{C,wall}} = \left[\max(0, F_{\text{C}}^{\text{d}} + F_{\text{C}}^{\text{c}}) \cdot \vec{n} \right] \quad (5)$$

$$J_{\text{N,wall}} = \left[\max(0, F_{\text{N}}^{\text{d}} + F_{\text{N}}^{\text{c}}) \cdot \vec{n} \right] \quad (6)$$

where F_{C}^{c} is the inclusion volume concentration transport flux, m/s, F_{N}^{C} is the inclusion number density transport flux, $1/(\text{m}^2 \text{ s})$, F_{C}^{d} is the inclusion volume concentration diffusion flux, m/s, F_{N}^{d} is the inclusion number density diffusion flux, $1/(\text{m}^2 \text{ s})$, $J_{\text{C,wall}}$ is the inclusion volume concentration wall adsorption flux, m/s, $J_{\text{N,wall}}$ is the inclusion number density wall adsorption flux, and \vec{n} is the normal vector.

The wall and entrance boundary conditions are shown in Table I.

Numerical Solution

In CFD calculations, the molten steel region is typically divided into several small control volumes or control surface components, resulting in a grid system that is utilized to define the fluid area in terms of physical issues as well as the fluid's features. Numerical computation models approximate the mathematical models underlying physical problems by solving these equations in each grid cell, simulating the flow of the entire fluid region. To establish a correlation between the two, the physical problem's boundary and beginning conditions are often applied to the grid model. The numerical calculation model then solves the related physical equations in each grid cell to determine the flow conditions across the entire fluid region. The governing equations are solved by the commercial software package CFX and the ANSYS-EMAG module, and the convergence was assumed to reach a point where all the normalized residuals are $< 10^{-5}$.

RESULTS AND DISCUSSION

Model Validation

Table II shows the physical model dimensions and calculation parameters of the tundish for model verification, which are consistent with the water model physical experiments. The temperature measurement system employs PT100 Platinum-Thermal resistance probes to monitor water temperature in the tundish with channel heating. These data are

Table I. Boundary conditions for inclusion transport

Parameter	Inclusion volume concentration	Inclusion number density
Inlet	C_0	N_0
Outlet	$\frac{\partial C}{\partial n} = 0$	$\frac{\partial N}{\partial n} = 0$
Tundish wall and free surface	$J_{C,wall}$	$J_{N,wall}$

Table II. Model and calculation parameters

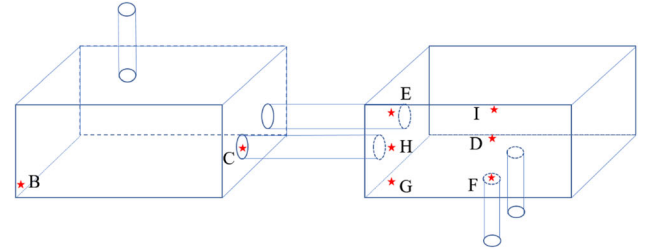
Parameters	Model tundish
Liquid	Water
Flow rate of the inlet	0.6984 (m ³ /h)
Depth of receiving chamber	240 (mm)
Depth of discharging chamber	350 (mm)
Length of receiving chamber	520 (mm) × 540 (mm)
Length of discharging chamber	540 (mm) × 540 (mm)
Length of channel	300 (mm)
Diameter of channel	60 (mm)
Power of single heating pipe	2.5 (kW)

captured by a paperless recorder. The specific temperature measurement points are shown in Fig. 2a: Point B is located at the lower left corner of the receiving chamber; Point C, at the channel inlet; Point D, centrally at the tundish exit; Point E, directly above the channel exit; Point F, at the tundish exit; Point G, underneath the channel exit; Point H, at the channel exit; Point I, above the tundish exit. UDV (ultrasonic Doppler velocimetry) is applied to measure the fluid velocity in the tundish. The measurement area is the velocity value of a section through the axial direction of the channel, the velocity points also intercept nine velocity points on the cross-section line for verification. The inclusion model is validated using a tundish capable of holding 35 tons of molten steel. The size and related parameters of the tundish are detailed in Table III, while the experimental sample is obtained from a 200-series stainless steel production in an industrial plant. In the numerical verification process, the initial inclusion concentration and number density are 271.5 ppm and $3.33 \times 10^{13}/\text{m}^3$.²⁴

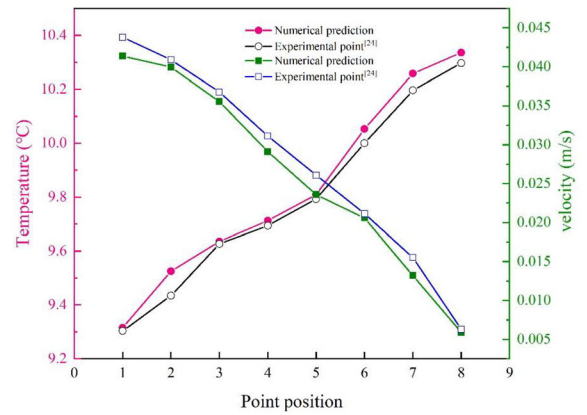
Figure 2b shows that the predicted results of velocity and temperature agree with the experimental data of the water model.²⁵ Figure 2c shows that the predicted values of inclusion number density agree well with the experimental data. The sample and slag are taken 300 mm below the pouring zone's slag layer and above the tundish outlet.

Inclusion Field Distribution Under Four Induction Heating Modes

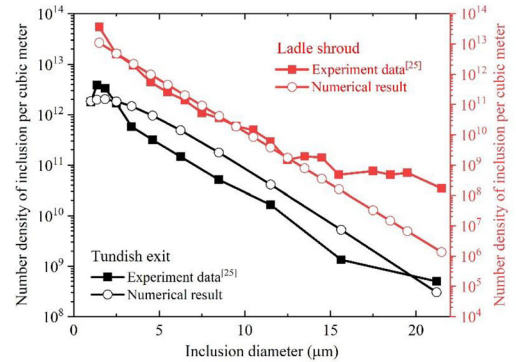
Figure 3 depicts the inclusion volume concentration distribution along the channel's longitudinal section, showing the following information: (1)



(a) The specific temperature measurement points



(b) Velocity and temperature measurements



(c) Inclusion number density of exit and ladle shroud

Fig. 2. Verification of tundish model.

Working conditions 1 and 3 have similar distribution shapes, and working conditions 2 and 4 have similar distribution forms. This similarity is primarily due to the flow mode and the dynamic process of collision and inclusion removal. A single flow behavior results in similar temperature field patterns, whereas the combination of two heat flow

Table III. Dimensions and parameters of model validation tundish and properties of molten steel

Parameters	Value
Tundish capacity	35 t
Number of strand	2 strands
Inlet velocity	0.81 (m/s)
Inlet temperature	1763 (K)
Density of molten steel	7020 (kg/m ³)
Heat capacity	750 (J/kg K)
Thermal conductivity	41 (W/m K)
Thermal expansion coefficient	1.0×10^{-4} (K ⁻¹)
Heat flux at the top surface	15 (kW/m ²)
Heat flux at the bottom wall	1.4 (kW/m ²)
Heat flux at the long walls	3.2 (kW/m ²)
Heat flux at the short walls	3.8 (kW/m ²)
Viscosity of molten steel	0.0067 (Pa s)
Diameter of the outlet	50 (mm)
Distance between the two outlets	4200 (mm)
Depth of the molten steel	925 (mm)

transport modes leads to different particle concentration fields. (2) Under working conditions 1 and 3, the channel failed to effectively remove inclusions, with minimal change in the concentration gradient, leading to a loss of functionality. In contrast, under working conditions 2 and 4, the concentration of inclusions decreased significantly, by approximately 50–70 ppm, demonstrating effective inclusion removal. The cause of the aforementioned issue is primarily multifaceted. The effectiveness of removal is determined by the fluid flow pattern in the pipe, collision frequency, transfer behavior and particle growth of inclusions in the channel. (3) The minimal volume concentration of inclusions is mostly concentrated at the discharging chamber's corners, where a high number of inclusions are absorbed and eliminated by the free surface.

Figure 4 depicts the spatial distribution of the density of inclusions. To begin, the numerical density of inclusions falls gradually from the receiving chamber to the discharging chamber. This is due to the removal of a significant number of inclusions, which collide with the particles as they grow, resulting in a decrease in the number of particles. Second, the number density gradient in the receiving chamber varies dramatically, with the majority of the density change occurring in the receiving chamber. The primary cause of this phenomenon is that the impact of the tundish's incoming flow is quite large, and particle collision happens almost immediately. Besides, object collisions are common, especially around the entrance to the bottom region. Finally, it is discovered that in working conditions 1 and 3, the number density of inclusions in the channel approaches the discharging chamber, whereas in working circumstances 2 and 4, the number density of inclusions in the channel is in a transitional stage. The number density of inclusions

in the receiving chamber is approximately one order of magnitude more than the number density of inclusions in the discharging chamber.

Figure 5 depicts the spatial field distribution of the characteristic radius of inclusions. Working conditions 1 and 3 show that the inclusions in the discharging chamber go through the bottom of chamber, disperse into the surroundings and then grow owing to the collision. The particle size of the inclusions at the channel's center decreases, and the free liquid surface in the discharging chamber increases. In working condition 1, the characteristic radius of inclusions in the discharging chamber shows a gradient increase from top to bottom. Working condition 3 exhibits a gradient change in the characteristic radius of inclusions in the middle area and corners of the discharging chamber.

The spatial distribution of the characteristic radius of inclusions is similar in working conditions 2 and 4. Near the entrance of the receiving chamber, the distribution is influenced by electromagnetic forces and shows a tendency for aggregation and growth towards the right. Changes within the channel are relatively mild. Additionally, the radius gradient changes very little, maintaining a fairly consistent shape.

Inclusion Field Characteristic Distribution

Figure 6 depicts the inclusion removal rate in each tundish chamber. It shows that the contribution of the inclusion removal rate is in the order of receiving chamber → discharging chamber → channel for operating conditions 1 and 3. Inclusion removal rates differ minimally between the receiving chamber and the discharging chamber. The contribution of the inclusion removal rate is in the order of receiving chamber → channel → discharging chamber in operating conditions 2 and 4. The inclusion removal rates in the channel are 27.58% and 26.49%, demonstrating that the two intermittent induction heating modes can significantly improve the dynamic conditions in the channel, especially in the inclusion removal process. However, for working condition 1, the channel has the least effective effect on inclusion removal, completely eliminating its metallurgical benefit. There is also significant variation in the discharging chambers, primarily influenced by the effectiveness of channel removal.

Figure 7 depicts the size of inclusions at various positions within the tundish. The particle size of inclusions for working conditions 1 and 3 increased in the channel by 0.51 μm and 0.7 μm , respectively. However, the large inclusions are not eliminated, causing them to flow into the crystallizer. The size of channel inclusions for working conditions 2 and 4 decreased by 0.86 μm and 0.81 μm , respectively. This is due to the dynamic environment and the removal of large inclusion particles in the distribution chamber. The size of inclusions that eventually

Numerical Simulation of Inclusion Collision Growth and Removal in a Tundish with Intermittent Induction Heating

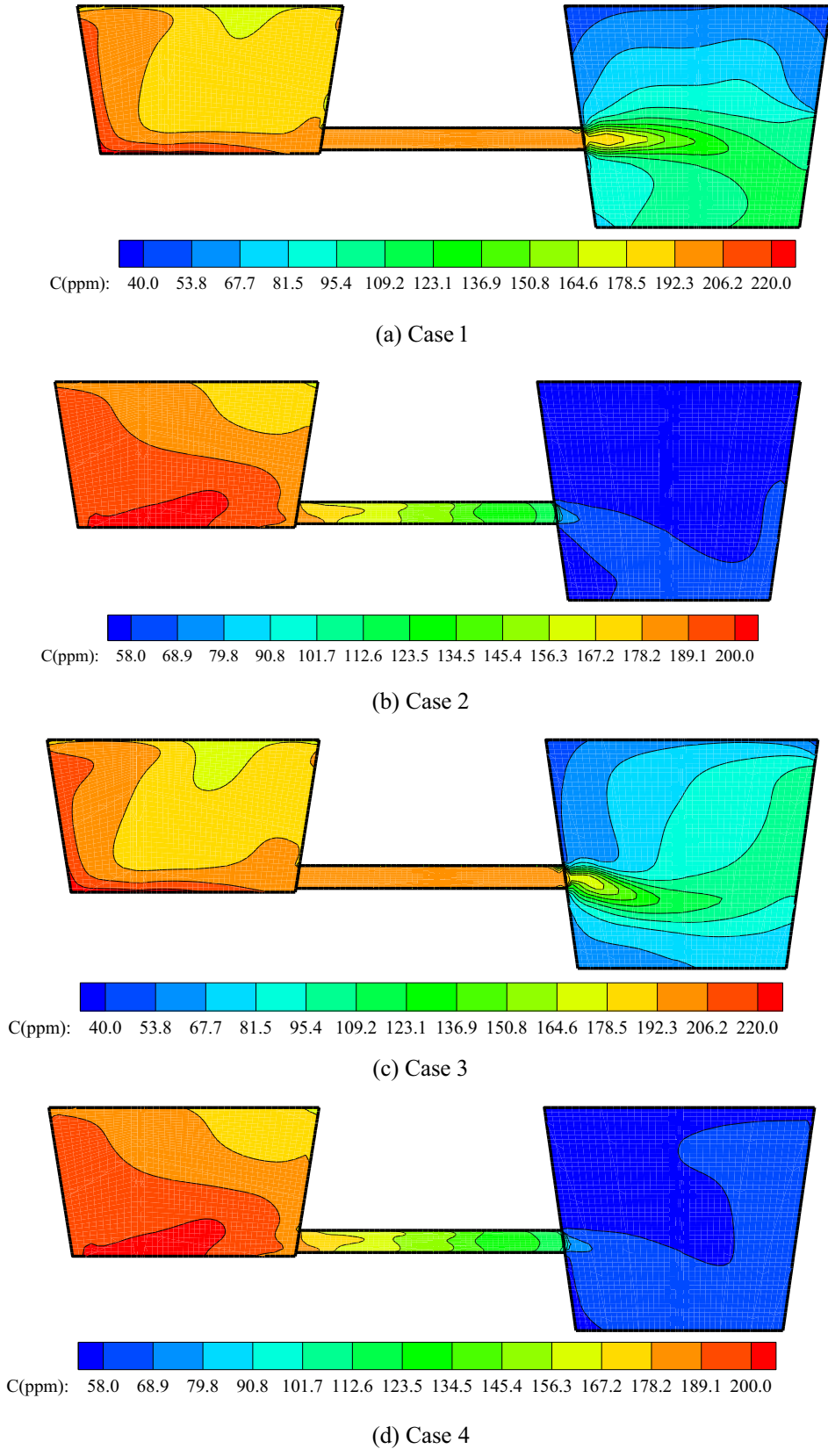
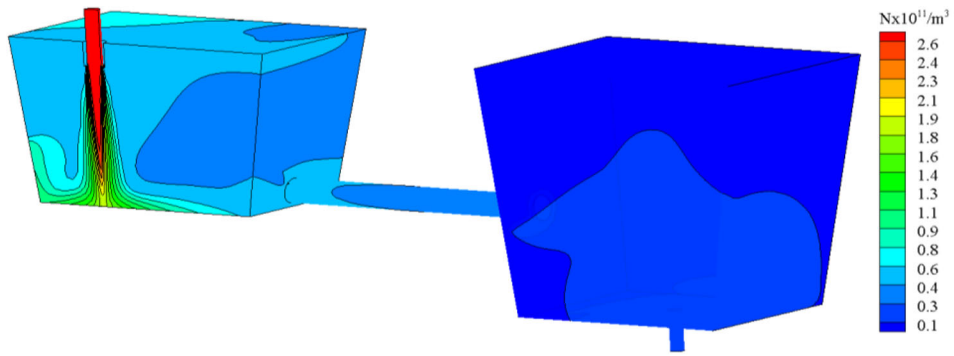
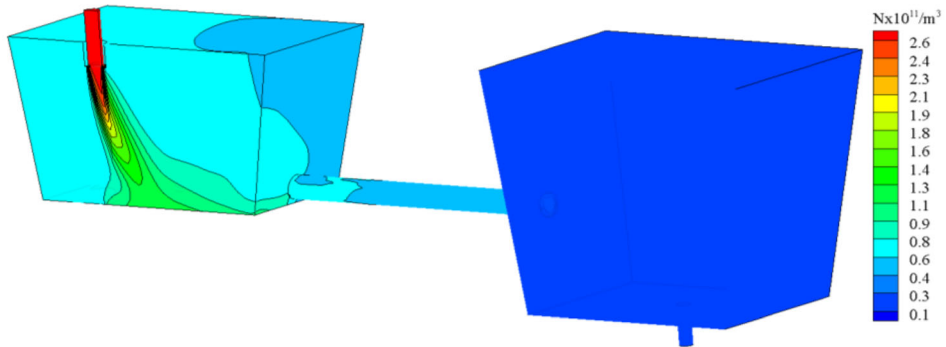


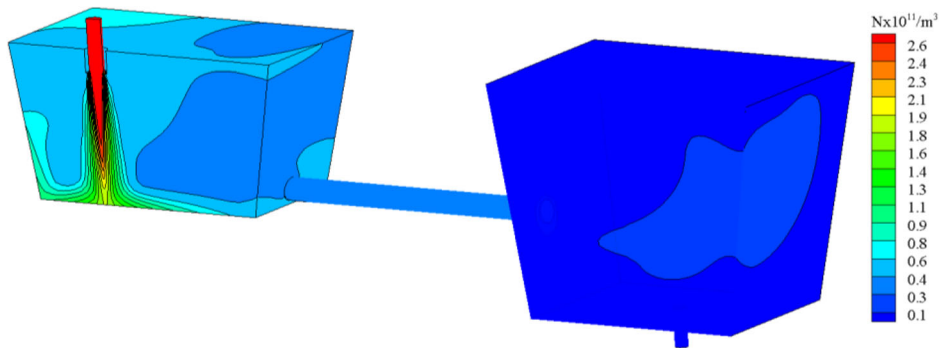
Fig. 3. Inclusion volume concentration field distribution through channel cross section.



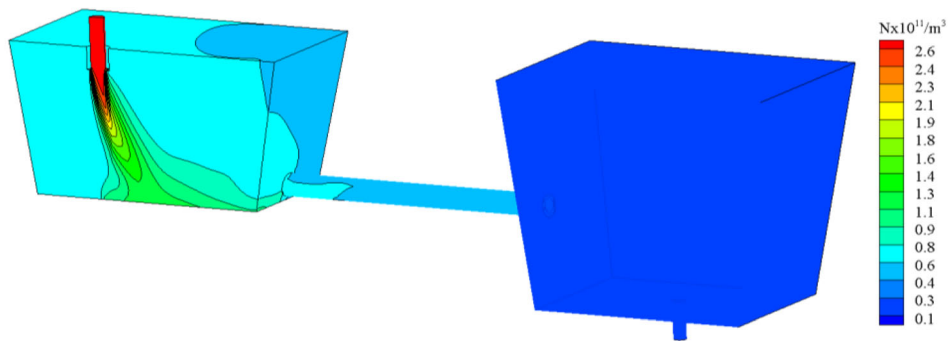
(a) Case 1



(b) Case 2



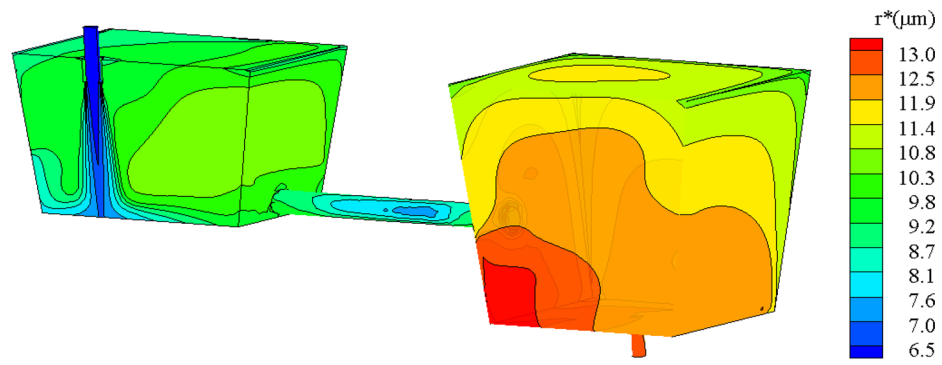
(c) Case 3



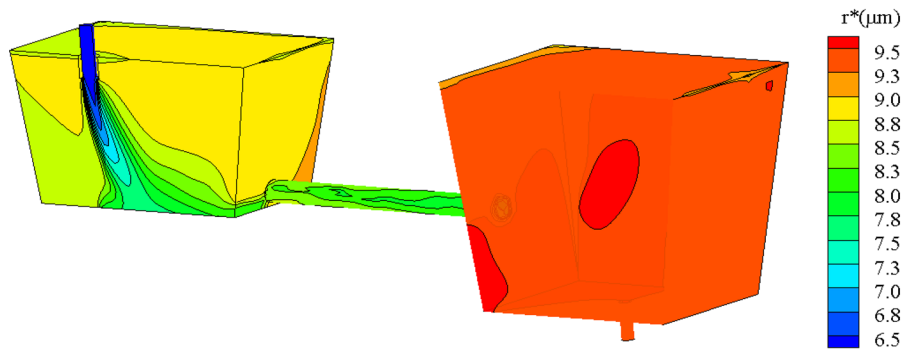
(d) Case 4

Fig. 4. Spatial field distribution of number density of inclusions.

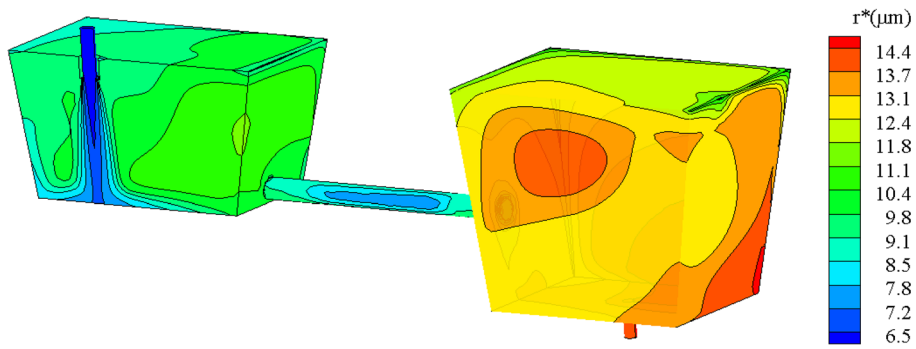
Numerical Simulation of Inclusion Collision Growth and Removal in a Tundish with Intermittent Induction Heating



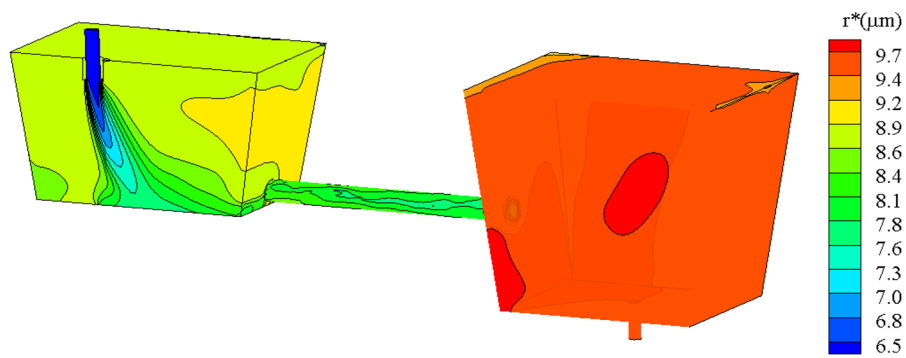
(a) Case 1



(b) Case 2



(c) Case 3



(d) Case 4

Fig. 5. Spatial field distribution of characteristic radius of inclusions.

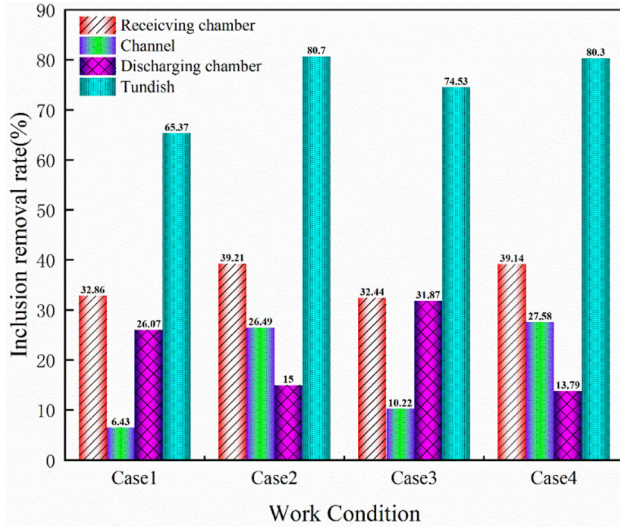


Fig. 6. Inclusion removal rate of each chamber in the reactor.

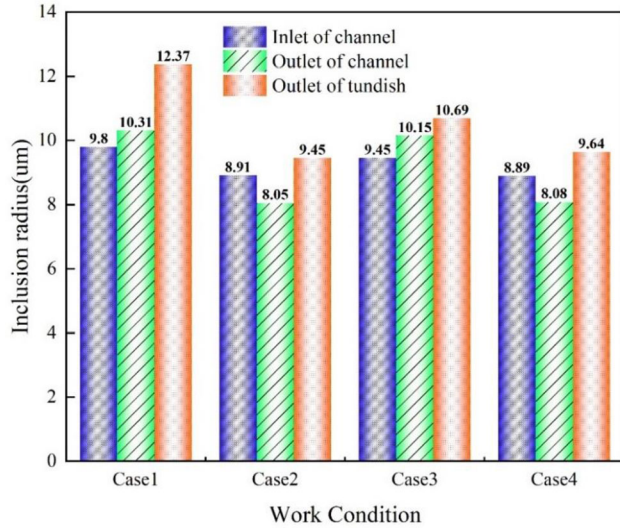


Fig. 7. Particle size of inclusions at characteristic positions in the reactor.

flow out of the tundish outlet is maintained at about $9.5 \mu\text{m}$, which is beneficial for the quality of the slab.

Table IV depicts the changes in inclusion removal rate at the tundish outlet at various time nodes throughout a cycle. The table shows that the inclusion removal rate from large to small is Case 2 \rightarrow Case 4 \rightarrow Case 3 \rightarrow Case 1. It can be observed that the inclusion removal rate does not correspond to the residence time. This is because, while residence time suggests that a longer period facilitates easier removal of inclusions, the floating removal of inclusions is not solely dependent on residence time. The removal rate of inclusions is also associated with broader characteristics such as inclusion particle size, spatial context and flow morphology. Additionally, the effect of electromagnetic force adds complexity to particle motion.

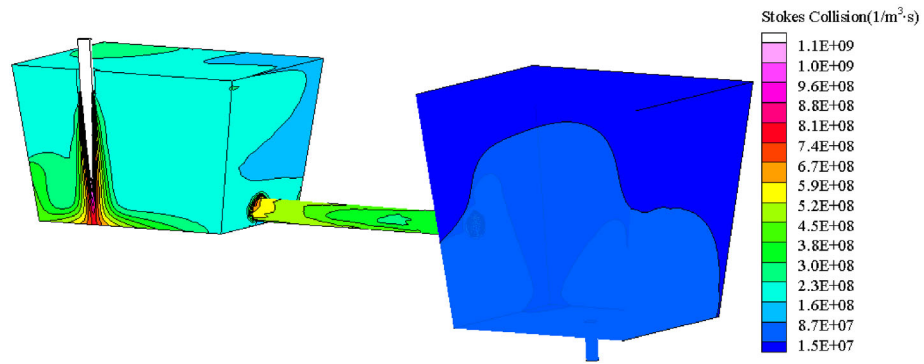
The spatial distribution of the contribution of Stoke collision to the inclusion number density source term with and without induction heating is given in Fig. 8a and b, which shows that without induction heating, the area with the greatest spatial distribution of the source term contribution is primarily concentrated in the vertical area of the shroud and channel inlet, owing to the highest fluid velocity, while with induction heating, the distribution below the shroud is deflected to the right because of the electromagnetic force, and the Stokes source term throughout the entire channel contributes significantly, suggesting that the spatial location leads to a strong collision of inclusions. Besides, the collision source term in the discharging chamber is relatively weak, with orders of magnitude far smaller than those in the receiving chamber and channel.

Figure 8c and d depicts the spatial distribution of the turbulent collision contribution to the inclusion number density source term with and without induction heating. It shows that without induction heating, the largest region of the turbulent collision source term is found at the bottom of the receiving chamber. Due to the high turbulent kinetic energy at this position, the collision source term is approximately 10^7 orders of magnitude larger, and the impact of the fluid hitting the bottom generates a stronger collision. Followed by the channel, the contribution of the turbulent collision source term rapidly decreases from the channel's entry to its departure. The contribution of the turbulent collision source term in the upper part of the

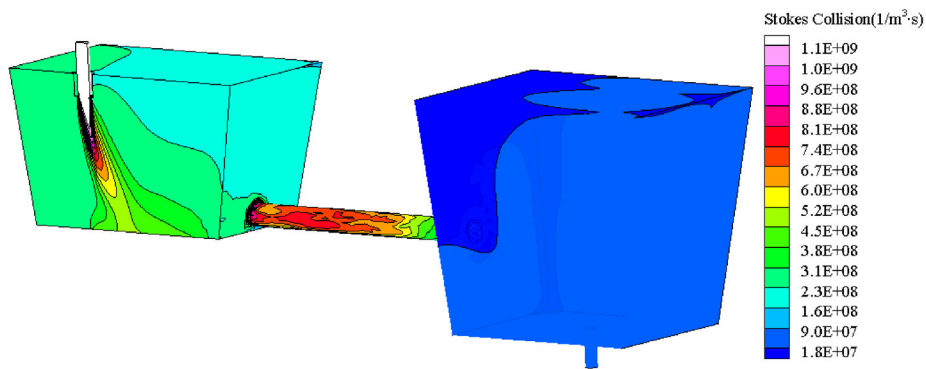
Table IV. Changes in the inclusion removal rate at the tundish outlet within a cycle

Cycle	Case 1 (%)	Case 2 (%)	Case 3 (%)	Case 4 (%)
1/8	0	0	0	0
2/8	55.47	70.07	70.07	70.07
3/8	66.13	64.01	64.01	79.87
4/8	65.60	81.2	73.17	63.10
5/8	65.43	64.83	80.27	76.37
6/8	65.40	81.07	80.12	72.3
7/8	65.37	65.13	63.17	73.27
1	65.37	80.7	74.53	80.3

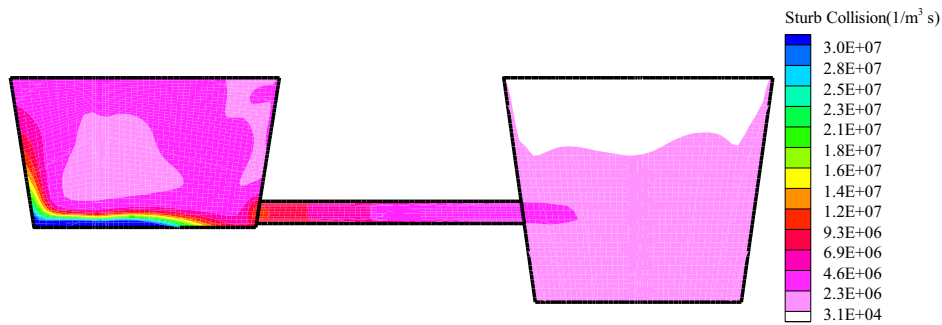
Numerical Simulation of Inclusion Collision Growth and Removal in a Tundish with Intermittent Induction Heating



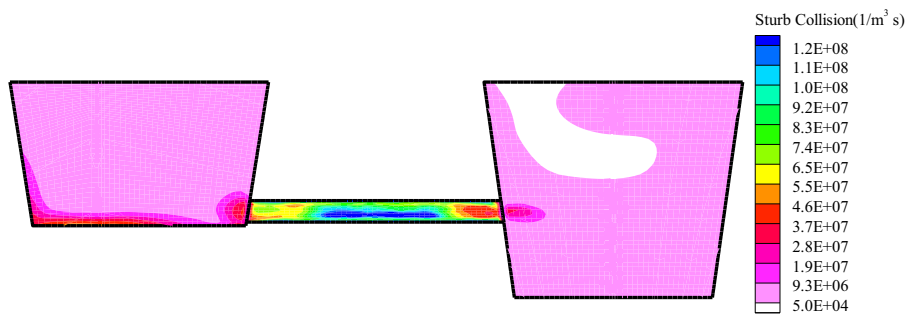
(a) without heating



(b) with heating



(c) without heating



(d) with heating

Fig. 8. Spatial distribution of Stoke collision and turbulent collision source term.

distribution chamber is the smallest, barely on the order of 10^4 . The flow in this location is generally gentle, and the turbulent kinetic energy is modest. However, with induction heating, the turbulent collision source term in the channel is the biggest, reaching the order of 10^8 , while the receiving and discharging chambers are relatively average at 1×10^7 ($1/m^3 s$). For the turbulent collision source term during induction heating, the term's overall order of magnitude is one order of magnitude higher than the turbulent collision source term without induction heating, and the difference within the channel is approximately two orders of magnitude.

Previous studies on inclusions in induction-heated tundishes have shown that the collision modes of inclusions are turbulence collision and electromagnetic collision^{19,22} due to the continuous nature of induction heating. In contrast, the collision modes of inclusions for intermittent induction heating include turbulent collision, Stokes collision (without induction heating) and electromagnetic collision (with induction heating). The latter two alternate, corresponding to the start and stop of induction heating.

Spatial Distribution of Inclusion Fields in Characteristic Areas

Table V displays the numerical features of the characteristic inclusion volume concentration and characteristic radius of the dead zone and non-dead zone areas. It indicates that (1) for the volume concentration of inclusions, the dead zone and the non-dead zone exhibit opposite tendencies, that is, the volume concentration of inclusions under working conditions 1 and 3 is lower in the dead zone and higher in the non-dead zone, while there is a reversal of the trend for working conditions 2 and 4. (2) Regarding the inclusion radius, the dead zone and non-dead zone have essentially the same properties. Working conditions 2 and 4 have a smaller inclusion radius, while working conditions 1 and 3 have a wider inclusion radius. As a result, the features of inclusions in the non-dead zone will influence the slab's overall quality. It is also a critical signal for assessing collision growth and

removal inside it. The dead zone acts as a flow stagnation zone, and the particle size has an impact on the overall system. The kinetic conditions and operational procedures enter the subsequent continuous casting process as well as the macroscopic distribution morphology in the metallurgical reactor.

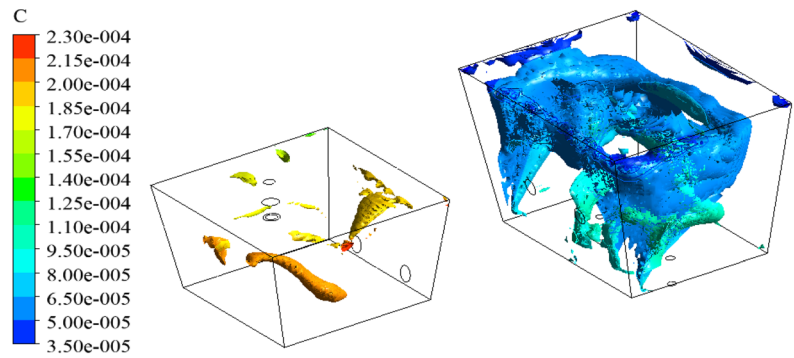
Figure 9 depicts the spatial distribution of inclusion concentration fields in the dead zone. The figure shows that the distribution of inclusion volume concentration in the dead zone differs between the four operating situations. The area with the highest inclusion concentration is concentrated in the receiving chamber's lower dead zone, whereas the area with the lowest inclusion concentration is concentrated in the discharging chamber's upper dead zone. Despite its slow flow, the volume concentration of inclusions in the dead zone is relatively modest. As a result, regional optimization is a good process and method based on production requirements. Besides, the three-dimensional spatial distribution within the dead zone clearly shows the issues produced by black box operations, and visualization is a critical method for displaying and evaluating detailed information.

Figure 10 depicts the spatial distribution of the characteristic radius of dead zone inclusions. The figure shows that for operating condition 1, the particle size distribution in the receiving and discharging chambers is uniform, with big particle inclusions primarily located in the bottom region of the dead zone. The particle radius distribution gradient is significant in working conditions 2 and 4, and large particle inclusions are mostly concentrated in the top area. The particle radius in the discharging chamber is primarily concentrated around $9.5 \mu m$, while it is mostly concentrated around $8.5 \mu m$ in the receiving chamber. Working condition 3 has a large distribution gradient due to the distinctive characteristics of its flow, and large inclusions are primarily located in the lower area. Consequently, the displayed size distribution of inclusions can show the local details and represent kinetic properties.

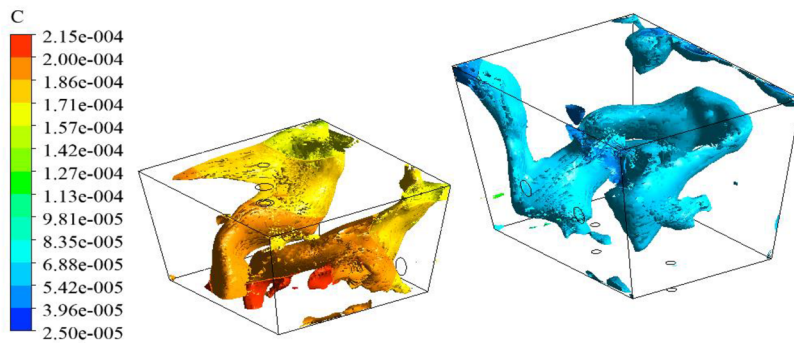
Table V. Characteristic inclusion volume concentration in the dead zone area

Cases	D_{ave} concentration (ppm)	D_{ave} radius (μm)	Non- D_{ave} concentration (ppm)	Non- D_{ave} radius (μm)
Case 1	72.3	11.8	149.67	10.63
Case 2	129.5	9.20	118.5	9.06
Case 3	108.9	13.3	147.4	11.53
Case 4	130.7	9.28	118.8	9.15

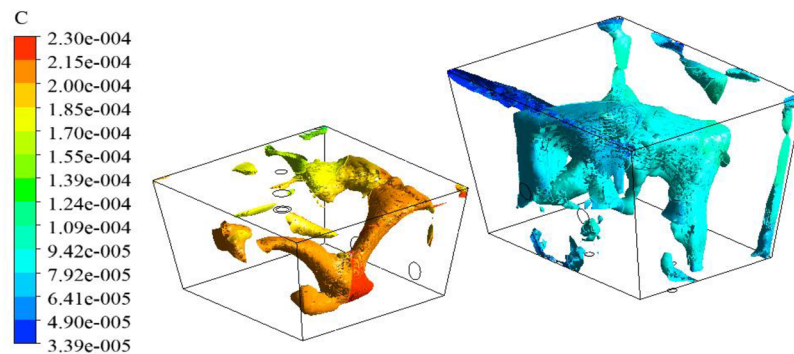
Numerical Simulation of Inclusion Collision Growth and Removal in a Tundish with Intermittent Induction Heating



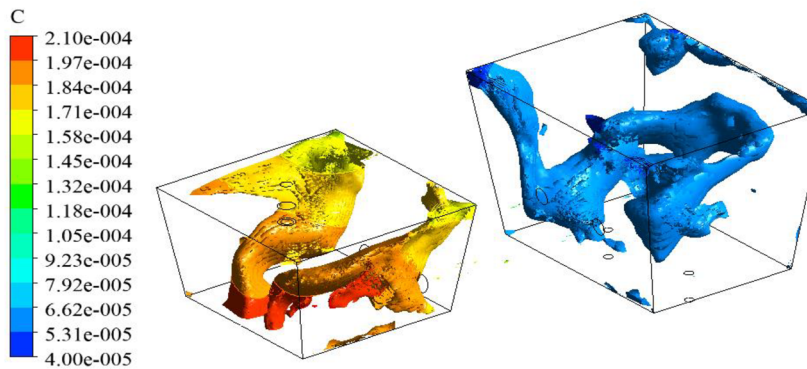
(a) Case 1



(b) Case 2

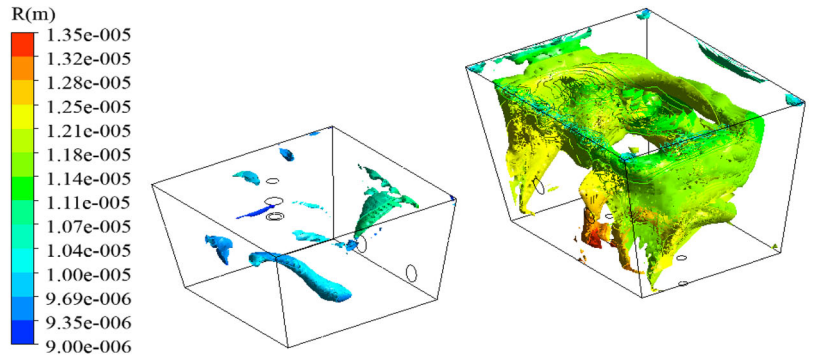


(c) Case 3

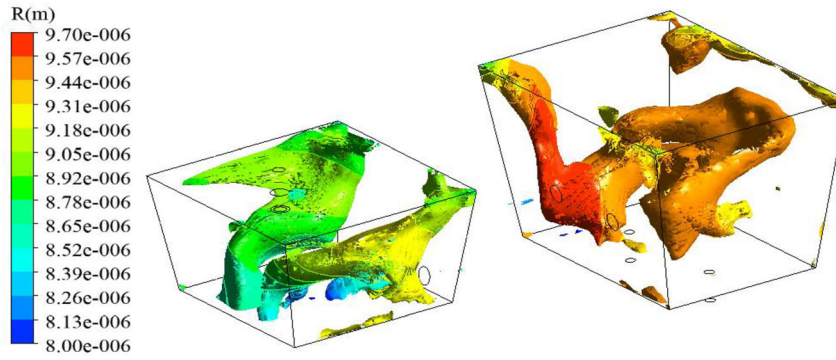


(d) Case 4

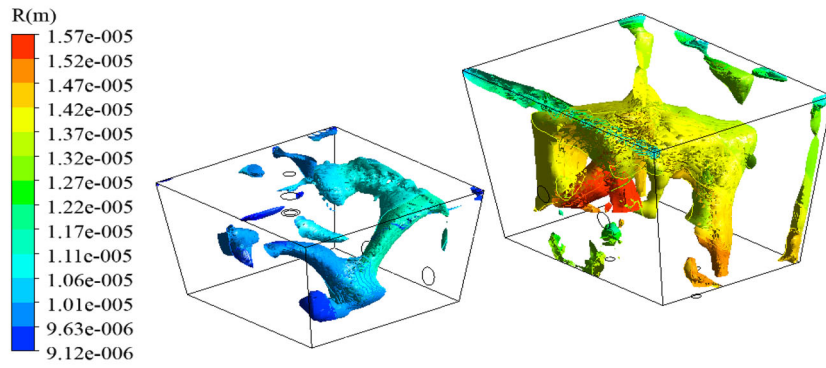
Fig. 9. Spatial distribution of inclusion concentration field in the dead zone.



(a) Case 1



(b) Case 2



(c) Case 3

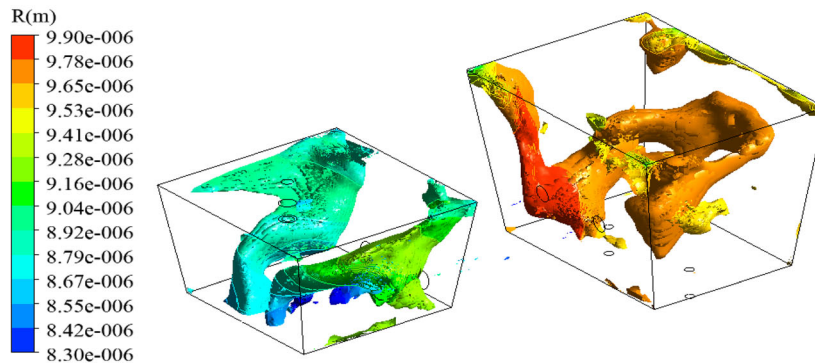


Fig. 10. Spatial distribution of characteristic radius of inclusions in the dead zone.

CONCLUSION

- (1) For high-frequency short heating with high-frequency short pause mode and mixed heating, the inclusion removal rates in the channel are 6.43% and 10.22%, respectively. For medium frequency medium heating with medium frequency medium pause mode and head-to-tail long heating mode, the inclusion removal rates in the channel are 27.58% and 26.49% respectively, indicating that the latter two modes improve inclusion removal in the channel, offering a viable option for inclusion removal in the tundish.
- (2) During induction heating, the turbulent collision source term in the channel is the largest, with its magnitude being one order higher than without induction heating and exhibiting a two-order magnitude difference within the channel. This suggests that induction heating primarily affects the slip velocity component in the collision process, increasing the collision frequency and thus accelerating the growth rate of inclusions.
- (3) For the half-way induction heating process, the induction heating modes of medium frequency medium heating and medium frequency medium pause mode and head-to-tail long heating mode can not only have a high inclusion removal rate and a small exit radius of the tundish but also a relatively uniform distribution of the inclusion field in the distribution chamber, which is consistent with the actual production requirements for inclusions to be dispersed in the molten steel. In actual production, the main function of the channel is to heat up and remove inclusions, and the two modes of tundish channels also achieve good results in the removal and radius of inclusions.
- (4) The characteristics of inclusions in the non-dead zone affect the slab's quality, serving as a crucial indicator for evaluating their collision growth and removal. The dead zone, a flow stagnation area, influences the macroscopic distribution shape in the metallurgical reactor and impacts the dynamics and operations of the subsequent continuous casting process. Therefore, understanding the dynamic relationship between internal fluids and inclusions in both dead and non-dead zones is essential for broader metallurgical reactor applications.

ACKNOWLEDGEMENT

Thanks to the University of Science Technology of Liaoning United Fund (HGSKL-USTLN(2022)07) for financial support.

CONFLICT OF INTEREST

The authors declare no conflict of interest.

REFERENCES

1. W.X. Dou, B.W. Zhang, Q. Yue, and H. Xiao, *Metalurgija* 59, 125 (2020).
2. Q. Zhang, G. Xu, and K. Iwai, *ISIJ Int.* 62, 56 (2022).
3. X. Qing, C. Hong, X.P. Wang, H. He, H.Y. Tang, and J.Q. Zhang, *Steel Res. Int.* 93, 2100839 (2022).
4. X.Q. Chen, P. Wang, H. Xiao, B. Yi, H.Y. Tang, and J.Q. Zhang, *J. Mater. Res. Technol.* 24, 1410 (2023).
5. H.Y. Tang, K.M. Wang, S.L. Xiao, J.W. Liu, and J.Q. Zhang, *Metals* 11, 1075 (2021).
6. Q. Yue, C.B. Zhang, and X.H. Pei, *Ironmak. Steelmak.* 44, 227 <https://doi.org/10.1080/03019233.2016.1209919> (2017).
7. L.F. Zhang, S.Q. Wang, Q.P. Dong, J.W. Gao, and L.N.W. Damoah, *Metall. Mater. Trans. B* 45, 2153 (2014).
8. S. Taniguchi and J.K.J.M. Brimacombe, *Magneto hydrodynamics* 32, 134 (1996).
9. K. Takahashi and S. Taniguchi, *ISIJ Int.* 43, 820 (2003).
10. Y. Sahai, *Metall. Mater. Trans. B* 47, 2095 (2016).
11. D. Mazumdar, *Steel Res. Int.* 90, 201800279 (2019).
12. S. Joo and R.I.L. Guthrie, *Metall. Trans. B* 24, 755 (1993).
13. K. Chattopadhyay, M. Isac, and R.I.L. Guthrie, *ISIJ Int.* 50, 331 (2010).
14. O.J. Ilegbusi and J. Szekely, *ISIJ Int.* 29, 1031 (1989).
15. Q. Wang, F.S. Qi, B.K. Li, and F. Tsukihashi, *ISIJ Int.* 54, 2796 (2014).
16. F. Xing, S.G. Zheng, Z.Q. Liu, and M.Y. Zhu, *Metals*. <http://doi.org/10.3390/met9050561> (2019).
17. F. Xing, S.G. Zheng, and M.Y. Zhu, *Steel Res. Int.* <https://doi.org/10.1002/srin.201700542> (2018).
18. H.Y. Tang, L.Z. Guo, G.H. Wu, H. Xiao, H.Y. Yao, and J.Q. Zhang, *Metals*. <https://doi.org/10.3390/met8060374> (2018).
19. H. Lei, B. Yang, Q. Bi, Y.Y. Xiao, S.F. Chen, and C.Y. Ding, *ISIJ Int.* 59, 1811 (2019).
20. W.X. Dou, Z.X. Yang, Z.M. Wang, and Q. Yue, *Metals* 11, 1536 <https://doi.org/10.3390/met11101536> (2021).
21. B. Yi, G.F. Zhang, Q. Jiang, P.P. Zhang, Z.H. Feng, and N. Tian, *Materials*. <https://doi.org/10.3390/ma16155254> (2023).
22. B. Yang, K. Liu, H. Lei, and P. Han, *High Temp. Mater. Process.* 41, 460 (2022).
23. D. Mazumdar and R.I.L. Guthrie, *ISIJ Int.* 39, 524 (1999).
24. H. Ling, L. Zhang, and H. Li, *Metall. Mater. Trans. B* 47, 2991 (2016).
25. B. Yang, H. Lei, Q. Bi, J.M. Jiang, H.W. Zhang, Y. Zhao, and J.A. Zhou, *Steel Res. Int.* 89, 1800173 (2018).

Publisher's Note Springer Nature remains neutral with regard to jurisdictional claims in published maps and institutional affiliations.

Springer Nature or its licensor (e.g. a society or other partner) holds exclusive rights to this article under a publishing agreement with the author(s) or other rightsholder(s); author self-archiving of the accepted manuscript version of this article is solely governed by the terms of such publishing agreement and applicable law.